Stability of stratified downslope flows with an overlying isolating layer

Arjun Jagannathan, Kraig Winters and Laurence Armi

Scripps Institution of Oceanography,
University of California San Diego
agjagann@ucsd.edu

Abstract

We investigate the dynamic stability of the analytically obtained downslope flow profiles of Winters and Armi (2014), characterized by an accelerating, stratified flowing layer beneath a homogeneous and stagnant isolating layer. We show that the inclusion of the isolating layer is an essential component of the stability analysis and further clarify the nature and mechanism of the instability in light of the wave-interaction theory. The spatial stability problem is also briefly examined in order to estimate the downstream location where finite amplitude features might manifest in streamwise slowly-varying flows over topography.

1 Introduction and background

Features reminiscent of overturning Kelvin-Helmholtz billows are often seen in the lee of topographically controlled stratified flows in the atmosphere and ocean. Despite a wealth of literature on the subject (e.g. Smith (1991), Scinocca and Peltier (1989), Farmer and Armi (1999), Armi and Mayr (2007) and references contained therein), the origin of these instabilities and their growth rate remain uncertain. Figure 1 shows the idealized spatial structure of the flows under consideration. A jet-like upstream profile with constant stratification, N_0 develops into a strong, thinning downslope flow beneath a layer of nearly stagnant, mixed fluid above that we call the isolating layer.

Shear instability was speculated to be the source of pulsations revealed in observations of the Boulder windstorm by Lilly (1978). However, spatial and temporal stability analysis of downslope flow solutions obtained from 2D numerical simulations of this flow (Peltier and Scinocca (1990)) as well as from earlier analytical solutions (Smith (1991)) severely underpredicted the growth rate and onset of instability.

Recently, Winters and Armi (2014) accounted for the upstream influence of the topography in constructing optimally-controlled, jet-like solutions that thin and accelerate over the crest. These solutions are valid in the asymptotic limit of tall topography and or slow flow/weak stratification and are characterized by blocking and the formation of a thinning accelerating jet below an isolating layer. Our objective here is to investigate the stability of these flow profiles at different downstream locations and examine whether the predictions are consistent with observed downslope flow pulsations.

2 A simple mathematical representation for downstream flow configurations

The upstream profile is a parabolic jet with an overlying dynamically uncoupled layer, each of height H for simplicity. The upstream buoyancy frequency is constant and equal to N_0. As the flow develops, at each downstream location, it remains quasi-jet-like, but with a reduced thickness $h = H - \delta_i$, a stronger stratification and an isolating layer of height δ_i. The volumetric flow rate, $Q = (2/3)U_0H$ upstream remains conserved. Next, we define

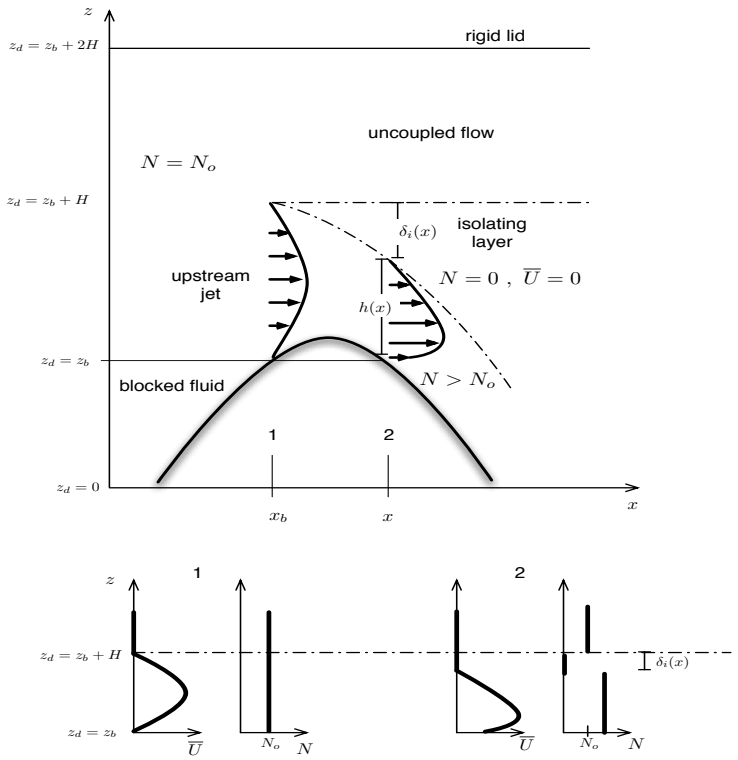

Figure 1: The downslope jet setting where flow configurations described above occur. The bottom panel displays the typical velocity and stratification profiles at the blocking point and an arbitrary point downstream of the crest, labelled 1 and 2 respectively.

$$\alpha = \frac{h}{H} = \frac{H - \delta_i}{H}, \tag{1}$$

and for ease of computation, at each α, we represent the flow mathematically as a superposition of a parabolic jet with maximum U_{δ_i} and a linear component that vanishes at $z_b + h$. Introducing a bottom velocity parameter β, the velocity of the bottom streamline in this representation is given by

$$u_b = \beta U_{\delta_i} \tag{2}$$

For different values of α, values of β and the fit they produced to the actual solutions of Winters and Armi (2014) are shown in figure 2. The velocity and density profiles are then given by,

$$\bar{U}_d(z_d) = \begin{cases} 0, & z_b + h \le z_d \le z_b + 2H, \\ 4U_{\delta_i}\left[\frac{z_d}{h} - \left(\frac{z_d}{h}\right)^2\right] + \frac{\beta U_{\delta_i}}{h}(h - z_d), & z_b \le z_d \le z_b + h. \end{cases} \qquad [m/s] \tag{3}$$

$$\bar{\rho}_d(z) = \begin{cases} \rho_0 + \Delta\rho - \frac{\Delta\rho}{2h} z_d, & z_b \le z_d \le z_b + h, \\ \rho_0 + \frac{\Delta\rho}{2}, & z_b + h \le z_d \le z_b + H, \\ \rho_0 + \frac{\Delta\rho}{2} - \frac{\Delta\rho}{2H}(z_d - H), & z_b + H \le z_d \le z_b + 2H, \end{cases} \qquad [kg/m^3] \tag{4}$$

where the overbar is used to denote the background flow field and the subscript 'd' indicates dimensional quantities. Note that Q conservation and the bottom velocity parameter β jointly determine the parabolic maximum U_{δ_i} at any given downstream position.

The above piecewise representations for the velocity and density introduce discontinuities in the derivatives of the velocity and density at $h(x)$ which are smoothed for numerical discretization purposes.

3 Mathematical formulation of the streamwise-local stability problems

The stability problem is developed using the primitive variable formulation and the normal mode decomposition in non-dimensional form. We investigate the stability of a steady parallel, stratified shear flow of the form, $\vec{u} = \bar{U}(z)\hat{\mathbf{i}}$; $\rho = \bar{\rho}(z)$ to 2D normal mode perturbations of the form,

$$(u', w', \rho', p') = (\hat{u}(z), \hat{w}(z), \hat{\rho}(z), \hat{p}(z))e^{ik(x-ct)}. \tag{5}$$

Substituting these in the inviscid Bousinnesq equations of motion and neglecting quadratic terms in the perturbation quantities, on a N_z sized grid, this can be shown to reduce to a $4N_z \times 4N_z$ generalized eigenvalue problem,

$$Av = cBv, \tag{6}$$

where A is a block diagonal matrix comprising 16 $N_z \times N_z$ blocks whose block entries depend on the background flow variables and the wave number k, B is a diagonal matrix and v is a column vector of the eigenfunctions.

From these, we may deduce the temporal growth rate

$$\omega_g^T = kc_i, \tag{7}$$

where the subscript i denotes imaginary part.

4 Numerical implementation

A Chebyshev pseudo-spectral collocation method is used to compute derivatives and construct the coefficient matrices. Boundary conditions of no normal flow $\hat{w}(z) = 0$ are imposed on the upper and lower boundaries. Note that the upper boundary is well above the location where the flowing layer meets the isolating layer and so the inflection point in $\bar{U}(z)$ at that location can affect the solutions.

5 Results

Note again that, with the present analytical representation, the values α and Q conservation completely determine the downstream flow profiles and define the stability problem. The optimal solution of Winters and Armi (2014) is characterized by an upstream parabolic jet with,

$$U_0 = (3/2)N_0H/\pi. \tag{8}$$

which can be easily shown to give a minimum Richardson number $Ri_{min} = \pi^2/36 > 1/4$, which is stable by the Miles-Howard theorem. At each subsequent downstream location, we solve the eigenvalue problem and extract the wave number k_{max} and phase speed c_r associated with the largest growth rate. Figure 3 displays the eigenfunctions $\|\hat{u}(z)|$ and $\|\hat{w}(z)|$ of the fastest growing unstable mode at each downstream location, and table 1 summarizes their characteristics.

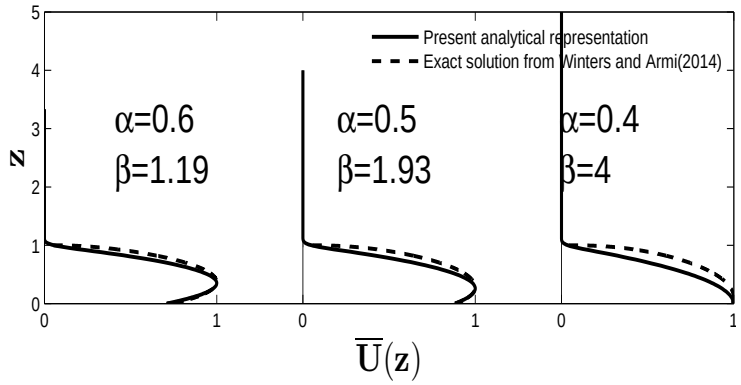

Figure 2: The Winters and Armi (2014) background velocity profiles at different downstream locations for the optimally controlled stratified downslope flow. The dashed lines are the exact solutions and the solid lines are the representations of these solutions using β and Q conservation.

.

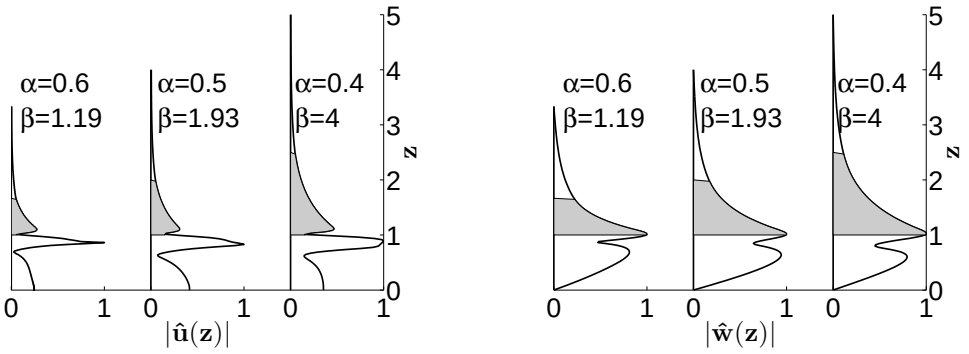

Figure 3: Normalized eigenfunctions (a)$|\hat{u}(z)|$ and (b)$|\hat{w}(z)|$ for the profiles representative of the solutions of Winters and Armi (2014).

Table 1: Characteristics of the unstable mode for the flow profiles representative of the exact solutions of Winters and Armi (2014)

α	β	k_{max}	ω_g^T	t_e	$L_e(=c_g/\omega_g^T)$	$T_p(secs)$	$\lambda(ms)$
0.66	0.89	4.0	0.0743	13.46	4.05	490	1933
0.64	1.00	3.6	0.0807	12.39	3.79	496	2083
0.62	1.09	2.8	0.0928	10.78	3.33	571	2595
0.6	1.19	2.8	0.1093	9.15	2.74	532	2520
0.5	1.94	2.0	0.1643	6.10	1.68	459	2930
0.4	4.00	1.6	0.1287	7.77	1.60	322	2930

1. k_{max} is the wave number of maximum temporal growth rate $\omega_g^T = \mathrm{Im}(k_{max}c)$.
2. t_e and L_e are the e-folding time and length for the fastest growing temporal and spatial mode, scaled by h/U_0 and h respectively.
3. c_g is the group velocity of the mode given by $c_g = \partial \mathrm{Re}(kc)/\partial k$

As the active layer crests the topography, the isolating layer increases in thickness, eventually triggering instability at a certain critical $\alpha_c \approx 0.66$. Downstream of this point, the growth rate appears to increase rapidly, growing to order $\mathcal{O}(10^{-1})$ at $\alpha_c \approx 0.6$. Thereafter a balance is attained between the increasing and weakening shears at $z = 1$ and $z = 0$ leaving the order of the growth rate unchanged. The $\mathcal{O}(1)$ e-folding times for the unstable modes are consistent with the non-linear simulations of Scinocca and Peltier (1989).

6 Discussion

Recall that Rayleigh's theorem gives the presence of an inflection point as a necessary condition for instability in a homogeneous shear flow. The flows examined above are essentially sheared flows endowed with an inflection point, but in a stably stratified environment. If shear were the driving mechanism of the instability, then we would expect stratification to have a stabilizing effect, modifying the unstable shear mode and reducing its growth rate.

Indeed we found that, for every flow configuration for which an unstable mode was present, the growth rate for the same shear profile, but without a stable stratification was larger. This identifies the unstable modes of table 1 as stratified analogues of inflectional Rayleigh modes, which we refer to as Kelvin-Helmholtz modes.

6.1 Physical interpretation of instability

The wave-interaction theory (see, e.g. Carpenter et al. (2011)) offers qualitative insight into the destabilizing mechanism at play. The key idea of the theory is that instability is possible whenever the flow configuration supports two or more waves whose direction of intrinsic propagation are of opposite signs. Additionally, for a large class of stratified flows, Baines and Mitsudera (1994) showed that an arbitrarily small region with $Ri < 1/4$, flanked on either side by regions where $Ri > 1/4$ is a sufficient condition for instability. Such a configuration effectively splits the flow into stable upper and lower waveguides, with no vertical wave propagation being possible in the central region. Two free modes in these separated waveguides can then interact to phase-lock and undergo mutual growth.

Figure 4a and 4b display the vorticity gradient and inverse Richardson number curves at the location $\alpha = 0.5$. The $\bar{U}_{zz}$ profile is seen to exhibit a large peak at $z = 1$ corresponding to the nearly discontinuous vorticity interface at the lower branch of the bifurcating streamline of figure 1. Below this, the values is constant, but reduced in strength and opposite in sign relative to the interface above. Thus the intrinsic direction of propagation of vorticity waves in each of these regions is opposite, satisfying one of the necessary conditions of the wave-interaction theory. The Baines and Mitsudera (1994) condition on the Ri profiles is also seen to be met.

However, the vorticity profiles exhibit only one distinct extremum; so the view of the instability as an interaction between two interfacial (or smeared) vorticity waves breaks down; and it is necessary to include the continuous spectrum in the analysis. Approximating $z = 1$ as a discontinuous shear interface, the speed of the rightward propagating vorticity wave here is given by, to first order

$$c_1 \approx \frac{\bar{U}_z|_{z=1^-}}{2k} \tag{9}$$

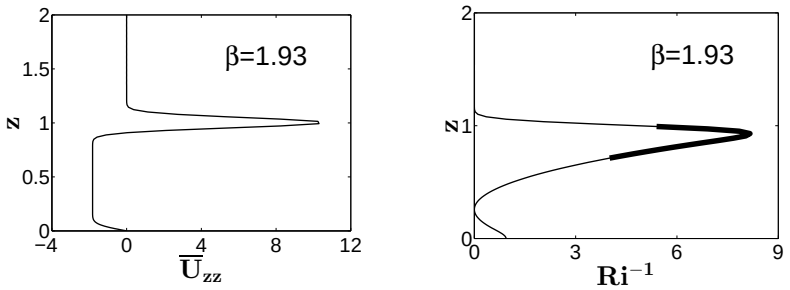

(a) (b)

Figure 4: (a) Vorticity gradient and (b) corresponding inverse Richardon number (Ri^{-1}) profile for the case $\alpha = 0.5$ and $\beta = 1.93$. The highlighted parts in (b) correspond to sub-quarter Ri regions. As the dynamically uncoupled layer is taken to be at rest, the vertical coordinate in the Ri^{-1} plot has been truncated at $z = 2$, the top of the isolating layer.

To circumvent the singularity of the 2D Taylor-Goldstein equation, we added a small amount of viscosity and diffusivity and solved the resulting 6th order equation for the stable flow profile revealed in the lower waveguide of figure 4b. Free slip and exponential decay conditions at the upper boundary filter the unstable Tollmien Schlichting waves. For the case $\alpha = 0.5, \beta = 1.93$, we found that at $k = 5$, there are two modes with speeds ≈ 0.26 which is roughly the same value that was found on applying Eq. 9 and which also matched the real part of the eigenvalue of the unstable mode that was found by solving the Taylor Goldstein equation for the complete profile

6.2 Spatial instability using the framework of Gaster (1962)

The discussion thus far has been restricted to temporal modes of instability. We now explore the spatial stability problem in an attempt to explain actual observed instabilities in downslope flows. We focus on the so-called signaling problem (Huerre et al. (2000)) which is the response of the flow to a localized periodic (in time) disturbance.

It is perhaps instructive to picture a curve of marginal stability (CMS),

$$\omega = f(k, \alpha, \beta) \tag{10}$$

for this problem, with ω being real valued on one side of the curve and complex on the other. As noted in section 5, the upstream flow, with $\alpha = 1, \beta = 0$ has $Ri_{min} > 1/4$, and the is thus stable. As the flowing layer begins to accelerate , Ri_{min} eventually drops below 1/4 allowing for the possibility of instability. The first location where a clear unstable mode is encountered is for $\alpha \approx 0.66$. It may thus be surmised that the point $(k, \alpha, \beta) = (4, 0.66, 0.89)$ in parameter space is close to the CMS for the flow. This in turn allows us to use Gaster's (1962) result that relates the growth rate of an unstable spatial mode to the corresponding temporal mode as,

$$k_g^s = -\omega_g^T / c_g, \tag{11}$$

where

$$c_g = \frac{\partial \omega_r}{\partial k} = \frac{\partial\ \mathrm{Re}(k c_r)}{\partial k} \tag{12}$$

is the group velocity of the temporal instability mode, which we compute numerically. Though strictly speaking, we have only argued that the first upstream unstable mode is

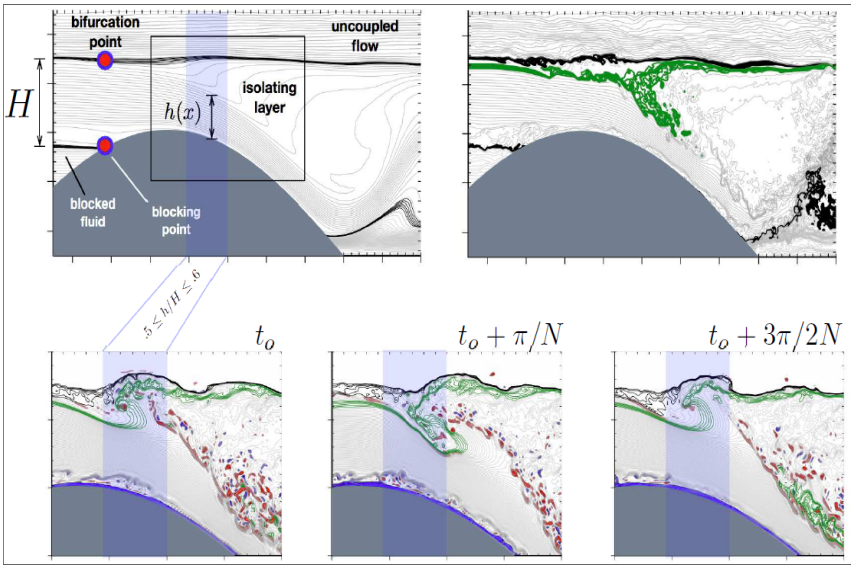

Figure 5: (Winters (2016)) Isopycnals and vorticity from a statistically steady non-linear simulation of stratified flow over a smooth topography matching the optimal upstream solution of Winters and Armi (2014). The top frame displays the time and cross-stream averaged flow (left) and an instantaneous snapshot (right). The bottom panel shows three snapshots of the flow spaced about half a buoyancy period apart and highlights the region $0.5 \leq h/H \leq 0.6$, where finite amplitude repeated overturning and plunging of the lower isopycnals (coloured green for visualization purposes) is visible. The red and blue colours indicate positive and negative vorticity extrema respectively.

close to the CMS, we use Eq. (11) to approximate the spatial growth rate at locations further downstream as well.

In table 1 we found the group velocity to be non-zero and positive in all cases, establishing them as convective modes. Thus we can define an e-folding length, $L_e = c_g/\omega_g^T$ which is the distance by which a growing mode propagates downstream as it undergoes amplification by a factor of e. The finite amplitude manifestation of instability typically occurs at a downstream position that is of the order of a few e-folding lengths.

6.3 Evolution to finite amplitude

If we define the horizontal length scale for the flow, $L_x \gg H$ as the distance over which the flowing layer height changes by 10%, then an interesting question is, at what downstream location can we expect to observe finite amplitude structures associated with the unstable spatial mode. An examination of the e-folding scales in table 1 suggests that even when the flow is 'just' hydrostatic with $L_x/H \approx 10$, the most upstream mode at $\alpha = 0.66$ with $L_e = 4.05h$ will have sufficient downstream distance to grow to $\exp 10/2.48 \approx 42$ times its initial magnitude before the background profile changes significantly at $\alpha \approx 0.56$. Thus we may expect to see finite amplitude K-H billows in the region $0.56 \leq \alpha \leq 0.66$

Recent work by Winters (2016) seems to corroborate this. Figure 5 shows the isopycnals from a statistically steady, 3D simulation of stratified flow over topography matching the optimal upstream solution of Winters and Armi (2014). The flow is seen to exhibit instability along the upper edge of the flowing layer, with finite amplitude repeated overturning and plunging billows manifesting within the shaded region $0.5 \leq h/H \leq 0.6$.

7 Conclusion

We have analyzed the linear stability of stratified flow profiles that match the theoretical downslope flow solutions of Winters and Armi (2014). We believe that it is the formal inclusion of the isolating layer into the stability analysis that is responsible for the dramatic improvement in the prediction of linear stability theory. The wave-interaction interpretation of shear flow instability appears to offer a satisfactory explanation for the observed instabilities. Further, for the spatial stability problem, applying Gaster's (1962) result is shown to yield $\mathcal{O}(1)$ e-folding length scales which signal transition to non-linearity at downstream distances consistent with those reported in observations and numerical simulations of downslope flows.

References

Armi, L. and Mayr, G. J. (2007). Continuously stratified flows across an alpine crest with a pass: shallow and deep föhn. *Q. J. R. Meteorol. Soc.*, 133(623):459–477.

Baines, P. G. and Mitsudera, H. (1994). On the mechanism of shear flow instabilities. *Journal of fluid mechanics*, 276:327–342.

Carpenter, J. R., Tedford, E. W., Heifetz, E., and Lawrence, G. A. (2011). Instability in stratified shear flow: Review of a physical interpretation based on interacting waves. *Appl. Mech. Rev.*, 64(6):060801.

Farmer, D. and Armi, L. (1999). Stratified flow over topography: the role of small-scale entrainment and mixing in flow establishment. In *Proc. R. Soc. London A*, volume 455, pages 3221–3258. The Royal Society.

Gaster, M. (1962). A note on the relation between temporally-increasing and spatially-increasing disturbances in hydrodynamic stability. *J. Fluid Mech.*, 14(02):222–224.

Huerre, P., Batchelor, G., Moffatt, H., and Worster, M. (2000). Open shear flow instabilities. *Perspectives in fluid dynamics*, pages 159–229.

Lilly, D. K. (1978). A severe downslope windstorm and aircraft turbulence event induced by a mountain wave. *J. Atmos. Sci.*, 35(1):59–77.

Peltier, W. and Scinocca, J. (1990). The origin of severe downslope windstorm pulsations. *J. Atmos. Sci.*, 47(24):2853–2870.

Scinocca, J. and Peltier, W. (1989). Pulsating downslope windstorms. *J. Atmos. Sci.*, 46(18):2885–2914.

Smith, R. B. (1991). Kelvin-Helmholtz instability in severe downslope wind flow. *J. Atmos. Sci.*, 48(10):1319–1324.

Winters, K. B. (2016). The turbulent transition of a supercritical downslope flow: sensitivity to downstream conditions. *Journal of Fluid Mechanics*, 792:997–1012.

Winters, K. B. and Armi, L. (2014). Topographic control of stratified flows: upstream jets, blocking and isolating layers. *J. Fluid Mech.*, 753:80–103.